Hindawi
Shock and Vibration
Volume 2022, Article ID 9721567, 10 pages
https://doi.org/10.1155/2022/9721567

Research Article

A Novel Structural Modification Method for Vibration Reduction: Stiffness Sensitivity Analysis with Principal Strain Application

Jiajun Hong and Takuya Yoshimura

Department of Mechanical Systems Engineering, Tokyo Metropolitan University, Tokyo 192-0397, Japan

Correspondence should be addressed to Jiajun Hong; hong-jiajun@ed.tmu.ac.jp

Received 28 July 2022; Accepted 5 November 2022; Published 16 November 2022

Academic Editor: Antonio Batista

This paper proposes a stiffness sensitivity analysis with principal strain application to decrease the out-of-plane vibration, which is the main source of the sound radiation of mechanical structures with thin plate parts. The sensitivity is evaluated as a differential coefficient of the target response with respect to the design variable, e.g., stiffness or mass. For suppressing the out-of-plane vibration, we pay attention to finding an appropriate location on the structure to add local stiffness. The location is decided according to stiffness sensitivity analysis results. The compliance frequency response function (FRF) is considered as the target response, and the thickness of stiffener is considered as the design variable. The validity of the proposed method is examined through numerical simulation with a finite element method (FEM) model of a thin plate. The modal principal strain distributions, stiffness sensitivity, and FRF changes by local thickening are calculated based on 4 selected natural modes. It is also examined by the experimental approach. The expected reduction of the response is attained by adding the stiffener (a thin stainless plate) to the appropriate location on the plate.

1. Introduction

For enhancing the passenger ride comfort of passenger vehicle, the requirement for reducing noise and vibration has increased gradually in recent years. Lightweight design is advocated for automobile production. Joost [1] showed that it can improve passenger vehicle fuel efficiency by 6–8% for each 10% reduction in weight. In pursuit of further light weighting, a great number of thin plates need to be used in vehicle components. Out-of-plane vibration of these thin plates is the main source of sound radiation [2, 3]. Vibration-proof and soundproof material can effectively reduce vibration and noise by attaching them to the thin plates, but they cannot be used for certain components, such as engine and drive components. Therefore, it is desirable to explore an efficient method to strike a balance between the lightweight design and noise and vibration performance of the structures. Experimental modal analysis (EMA) is an effective instrument for describing, understanding, and modelling the dynamic behaviour of a structure. EMA is considered reliable because it is based on input-output system identification, which allows validation of the estimated frequency response functions (FRFs) by coherence functions [4]. To date, considerable research studies based on EMA have been conducted for structure modification. Kim proposed a practical method to reduce a medium size test car's interior noise by using the experimental structural-acoustic modal coupling coefficient [5]. Terada and Yoshimura proposed a power spectrum sensitivity analysis for the noise reduction under operational condition without using input identification [6]. Ye et al. studied a systematic analysis methodology based on classical transfer path analysis for analyzing and reducing the low-frequency vibration of steering wheel [7]. Nakamura et al. proposed a stiffness sensitivity analysis on a panel by using the angular displacement response estimated by a scanning laser doppler vibrometer [8]. However, it is hard to use the scanning laser Doppler vibrometer on a complex surface of general structures. So, we considered the possibility of replacing the scanning laser Doppler vibrometer. The piezoelectric strain sensor is widely used in structural damage detection for measuring modal strain. Tsurumi et al. proposed a method

to detect structural damage based on modal strain energy in 1993 [9]. Doebling et al. used piezoelectric strain sensors in methods of implementing state estimate feedback to aid in damage detection in smart structures [10]. Given its small size, excellent performance, and the ability to cope with complex surfaces, we thought of replacing the Doppler vibrometer with a piezoelectric strain sensor. In the previous research, Yamada et al. tried to conduct a sensitivity analysis based on strain measurement effectively to reduce the vibration of the structure. The results show the effectiveness of Yamada's work in bending modes, but it is difficult to apply in twisting modes [11]. In this work, a stiffness sensitivity analysis with principal strain measurement is proposed to decrease the out-of-plane vibration of structure in both bending and twisting modes. The piezoelectric strain sensors were used to widen the applicable scope of sensitivity analysis. FEM simulation and experiment approach were conducted for confirming the proposed stiffness analysis method. The results verified the effectiveness of the method.

2. Sensitivity Analysis Theory

Calculation of the derivatives of the target response with respect to the design variables is called sensitivity analysis. The plus-minus sign of the sensitivity value represents the increment-decrement effect of the target response by changing the design variables. It enables us to determine the optimal modification locations on the target mechanical structure. By changing the design variables, e.g., stiffness or mass, at an appropriate location, effective reduction can be achieved on the target response at a specific frequency.

2.1. Stiffness Sensitivity Analysis with Strain Measurement. The FRF between the excitation point f and the response point r will be changed by adding the local additional stiffness Δk between points i and j on the structure as shown in Figure 1.

The change in FRF G_{rf} by local additional stiffness is

$$\begin{aligned}\Delta G_{\mathrm{rf}} &= \begin{bmatrix} G_{\mathrm{ri}} & G_{\mathrm{rj}} \end{bmatrix} \begin{bmatrix} \Delta k & -\Delta k \\ -\Delta k & \Delta k \end{bmatrix} \begin{bmatrix} G_{\mathrm{if}} \\ G_{\mathrm{jf}} \end{bmatrix} \\ &= -\Delta k \left(G_{\mathrm{ri}} - G_{\mathrm{rj}}\right)\left(G_{\mathrm{if}} - G_{\mathrm{jf}}\right),\end{aligned} \tag{1}$$

where Δk is the additional stiffness, G is the compliance FRF, and the subscript "rf" indicates the response point "r" and the excitation point "f" relatively.

When the addition stiffness Δk is small enough, the stiffness sensitivity S_k can be estimated by

$$S_k = \frac{\partial G_{\mathrm{rf}}}{\partial k} = -\left(G_{\mathrm{ri}} - G_{\mathrm{rj}}\right)\left(G_{\mathrm{if}} - G_{\mathrm{jf}}\right). \tag{2}$$

When the research target is a plate-like structure as shown in Figure 2, the compliance FRFs for estimating sensitivity can be approximately replaced by angular displacement FRF, and stiffness sensitivity can be expressed as

$$S_k = \frac{\partial G_{\mathrm{rf}}}{\partial k} = -t^2\left(\theta_{\mathrm{ri}} - \theta_{\mathrm{rj}}\right)\left(\theta_{\mathrm{if}} - \theta_{\mathrm{jf}}\right), \tag{3}$$

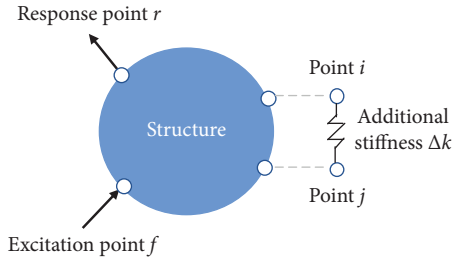

Figure 1: Measurement points and additional stiffness on the structure.

where t is the distance from stiffness modification surface to neutral surface of the structure.

Since it is difficult to measure angular displacement on the structure, application of strain measurement is explored in this work. Since the distance from the stiffness modification surface to the neutral surface does not change during deformation, vertical strain can be ignored throughout the plate. It is assumed that the strains between points i and j are uniformly distributed and can be expressed as

$$\varepsilon_{ij} = t\frac{\theta_i - \theta_j}{b}, \tag{4}$$

where b is the distance between points i and j, namely, the length of the stiffener attached to the structure.

Additional stiffness Δk due to stiffener is calculated by

$$\Delta k = \frac{\Delta AE}{l} = \frac{a\Delta tE}{b}, \tag{5}$$

where a is the width of the stiffener; ΔA is the added stiffener section area; and Δt is the added stiffener thickness.

Substituting (4) and (5) into (3), the sensitivity analysis with respect to bending stiffness by using the strain measurement can be formulated as

$$S_t = \frac{\partial G_{rf}}{\partial t} = -abE\varepsilon_{ir}\varepsilon_{if}. \tag{6}$$

In the condition of structure under dominant bending mode, since the modal maximum principal strains distribute along the direction vertical to the bending line on the surface and the minimum principal strains are too small to be ignored, Equation (6) is accessible (this will be verified in the numerical simulation part). But when structure under dominant twisting mode, both the principal maximum and minimum strains cannot be ignored, so it is necessary to consider X and Y-direction strains since the principal strains are criss-cross distributed on the surface. The sensitivity formulation is expressed as

$$S_t = -abE\left(\varepsilon_{x,ir}\varepsilon_{x,if} + \varepsilon_{y,ir}\varepsilon_{y,if}\right), \tag{7}$$

where the subscripts "x," "y" indicate the strain in x-direction and y-direction relatively. By the way, the strain value that can most accurately reflect the sensitivity characteristics of a certain point is the principal strain. The detailed calculation formula will be described in detail below.

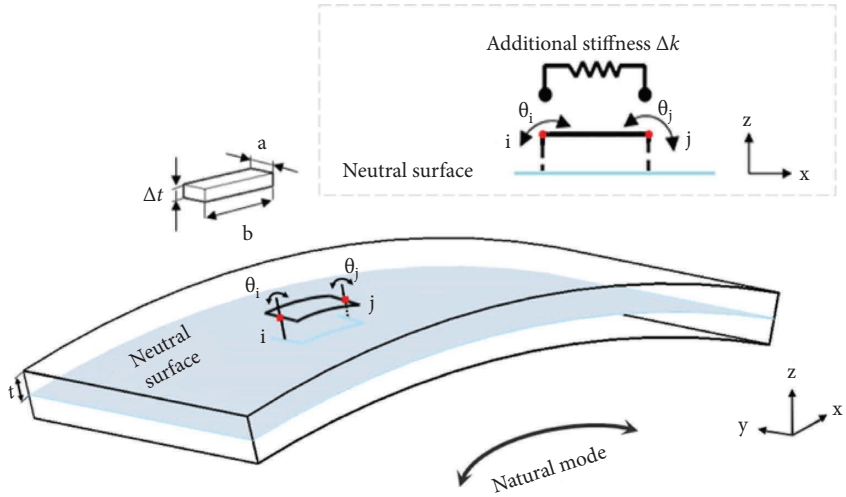

Figure 2: Measurement points and stiffener on the plate-like structure under natural mode.

In fact, the sensitivity estimated by the above equations cannot directly evaluate the increment-decrement effect since its value is a complex number. To evaluate the increase and decrease of the FRF amplitude by sensitivity, the vector projection of sensitivity onto FRF is used to convert sensitivity value to a real number at a specific frequency [12]. The sensitivity projection is estimated by the following equation:

$$S' = \mathrm{Re}\left(\frac{G_{rf}^{\mathrm{conj}} \bullet S}{\left|G_{rf}\right|}\right), \tag{8}$$

where Re() indicates real parts, superscript "conj" indicates complex conjugates, and S is the sensitivity estimated by equation (6).

2.2. Mass Sensitivity. It needs to be considered that as additional stiffness increases, additional mass effects will also arise. To properly evaluate the proposed sensitivity analysis by using the strain measurement, mass sensitivity analysis should also be carried out. By calculating the derivatives of the out-of-plane compliance FRF with respect to additional mass, adding the stiffener to the location with large mass sensitivity can be avoided. Mass sensitivity is estimated by [13]

$$S_m = \frac{\partial G_{\mathrm{rf}}}{\partial m} = \omega^2 G_{\mathrm{ri}} G_{\mathrm{if}}, \tag{9}$$

where ω is the angular frequency.

2.3. Modal Strains. In this study, the strains of surfaces and the out-of-plane displacement $w(x, y)$ of a thin plate with small deflection can be expressed by equation (9) [14].

$$\varepsilon = \begin{Bmatrix} \varepsilon_x \\ \varepsilon_y \\ \gamma_{xy} \end{Bmatrix} = -z \begin{Bmatrix} \dfrac{\partial^2 w}{\partial x^2} \\ \dfrac{\partial^2 w}{\partial y^2} \\ \dfrac{\partial^2 w}{\partial x \partial y} \end{Bmatrix}, \tag{10}$$

where z is the distance from the stiffness modification surface to the neutral surface of the structure.

Fourth-order polynomial expressions are conveniently used to define the shape functions with 12 parameters as shown in equation (10).

$$w = \alpha_1 + \alpha_2 x + \alpha_3 y + \alpha_4 x^2 + \alpha_5 xy + \alpha_6 y^2 + \alpha_7 x^3 + \alpha_8 x^2 y + \alpha_9 x y^2 + \alpha_{10} y^3 + \alpha_{11} x^3 y + \alpha_{12} x y^3 \equiv \mathbf{P}\boldsymbol{\alpha}, \tag{11}$$

where $\mathbf{P} = (1, x, y, x^2, \mathrm{xy}, \mathrm{y}^2, x^3, x^2 y, x\mathrm{y}^2, \mathrm{y}^3, x^3 y, x\mathrm{y}^3)$ and α is the parameter vector containing unknown twelve constants α_1 to α_{12}.

Substituting coordinate values into (10), the constants α_1 to α_{12} can be evaluated by the 12 simultaneous equations linking the values of out-of-plane displacement and rotations (w, θ_x, θ_y) of each element.

List all 12 equations, and (10) can be written in matrix form as

$$\tilde{\mathbf{u}}^{\mathbf{e}} = \mathbf{C}\boldsymbol{\alpha}, \tag{12}$$

where $\mathbf{C}$ is a 12×12 matrix depending on nodal coordinates. Substituting (11) into (10), out-of-plane displacement can be expressed as

$$\mathbf{w} = \mathbf{P}\mathbf{C}^{-1}\tilde{\mathbf{u}}^{\mathbf{e}}, \tag{13}$$

where $\tilde{\mathbf{u}}^{\mathbf{e}}$ is a vector consisting of the nodal displacements and rotations of the element.

Substituting (12) into (9), the strain vector at the element surface can be expressed by

$$\boldsymbol{\varepsilon} = -z\mathbf{B}\tilde{\mathbf{u}}^{\mathbf{e}}, \tag{14}$$

where $\mathbf{B}$ is the strain matrix of the element containing the second derivatives of the shape functions. Therefore, the modal strains $\phi_{\varepsilon}^{\mathbf{e}}$ on the surface of the element can be expressed as

$$\boldsymbol{\phi}_{\boldsymbol{\varepsilon}}^{\mathbf{e}} = -z\mathbf{B}\boldsymbol{\phi}^{\mathbf{de}}, \tag{15}$$

where $\phi^{\mathbf{de}}$ is modal displacement of the element.

2.4. Modal Principal Strains

2.4.1. Numerical Modal Principal Strains. In the numerical approach, the r^{th} modal principal (maximum and minimum) strains of the n^{th} element $(\phi_{\varepsilon}^{1,2})_{\mathbf{nr}}$ can be expressed as [15]

$$\left(\boldsymbol{\phi}_{\boldsymbol{\varepsilon}}^{1,2}\right)_{\mathbf{nr}} = \frac{\left(\boldsymbol{\phi}_{\boldsymbol{\varepsilon}}^{\mathbf{x}}\right)_{\mathbf{nr}} + \left(\boldsymbol{\phi}_{\boldsymbol{\varepsilon}}^{\mathbf{y}}\right)_{\mathbf{nr}}}{2} \pm \sqrt{\left[\frac{\left(\boldsymbol{\phi}_{\boldsymbol{\varepsilon}}^{\mathbf{x}}\right)_{\mathbf{nr}} - \left(\boldsymbol{\phi}_{\boldsymbol{\varepsilon}}^{\mathbf{y}}\right)_{\mathbf{nr}}}{\mathbf{2}}\right]^{2} + \left[\frac{\left(\boldsymbol{\phi}_{\boldsymbol{\varepsilon}}^{\mathbf{xy}}\right)_{\mathbf{nr}}}{\mathbf{2}}\right]^{2}}, \tag{16}$$

where $(\phi_{\varepsilon}^{\mathbf{x}})_{\mathbf{nr}}$, $(\phi_{\varepsilon}^{\mathbf{y}})_{\mathbf{nr}}$, and $(\phi_{\varepsilon}^{\mathbf{xy}})_{\mathbf{nr}}$ are the r^{th} modal strains of the n^{th} element in the x-direction, y-direction, and shear strain. They can be achieved by equation (14).

Principal angle (a counterclockwise direction from x axis to principal strain axis) can be expressed as

$$\left(\boldsymbol{\phi}_{\mathbf{P\_S}}\right)_{\mathbf{nr}} = \frac{1}{2}\tan^{-1}\frac{\left(\boldsymbol{\phi}_{\boldsymbol{\varepsilon}}^{\mathbf{xy}}\right)_{\mathbf{nr}}}{\left(\boldsymbol{\phi}_{\boldsymbol{\varepsilon}}^{\mathbf{x}}\right)_{\mathbf{nr}} - \left(\boldsymbol{\phi}_{\boldsymbol{\varepsilon}}^{\mathbf{y}}\right)_{\mathbf{nr}}}. \tag{17}$$

2.4.2. Experimental Modal Principal Strains. In the experimental approach, triaxial rosette strain gauge arrangement can be used. The arrangement of three strain gauges is shown in Figure 3 [16]. Instead of conventional strain gauges, piezoelectric strain sensors are used for modal response measurement.

The r^{th} modal principal (maximum and minimum) strains of the n^{th} element $(\phi_{\varepsilon}^{1,2})_{\mathbf{nr}}$ can be expressed as

$$\left(\boldsymbol{\phi}_{\boldsymbol{\varepsilon}}^{1,2}\right)_{\mathbf{nr}} = \frac{\left(\boldsymbol{\phi}_{\boldsymbol{\varepsilon}}^{1}\right)_{\mathbf{nr}} + \left(\boldsymbol{\phi}_{\boldsymbol{\varepsilon}}^{2}\right)_{\mathbf{nr}}}{2} \pm \sqrt{\left[\frac{\left(\boldsymbol{\phi}_{\boldsymbol{\varepsilon}}^{1}\right)_{\mathbf{nr}} - \left(\boldsymbol{\phi}_{\boldsymbol{\varepsilon}}^{3}\right)_{\mathbf{nr}}}{\mathbf{2}}\right]^{2} + \left[\frac{\left(\boldsymbol{\phi}_{\boldsymbol{\varepsilon}}^{2}\right)_{\mathbf{nr}} - \left(\boldsymbol{\phi}_{\boldsymbol{\varepsilon}}^{3}\right)_{\mathbf{nr}}}{\mathbf{2}}\right]^{2}}, \tag{18}$$

where $(\phi_{\varepsilon}^{1})_{\mathbf{nr}}$, $(\phi_{\varepsilon}^{2})_{\mathbf{nr}}$, and $(\phi_{\varepsilon}^{3})_{\mathbf{nr}}$ are the r^{th} modal strains of the n^{th} element in the 1, 2, and 3 directions, respectively.

Principal angle (counterclockwise direction from 1 axis to principal strain axis) can be expressed as

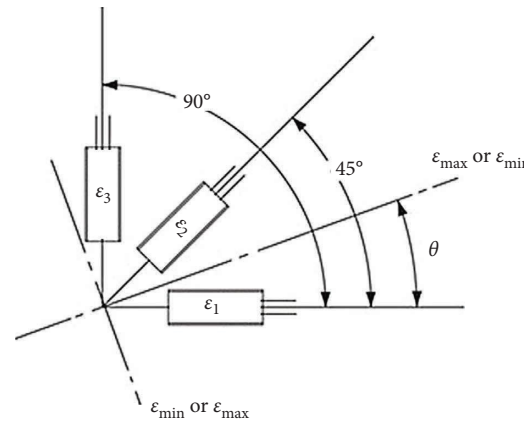

Figure 3: Triaxial rosette piezoelectric strain sensor arrangement [16].

$$\left(\boldsymbol{\phi}_{\mathbf{P\_E}}\right)_{\mathbf{nr}} = \frac{\mathbf{1}}{\mathbf{2}}\tan^{-1}\frac{2\left(\boldsymbol{\phi}_{\boldsymbol{\varepsilon}}^{3}\right)_{\mathbf{nr}} - \left[\left(\boldsymbol{\phi}_{\boldsymbol{\varepsilon}}^{1}\right)_{\mathbf{nr}} + \left(\boldsymbol{\phi}_{\boldsymbol{\varepsilon}}^{2}\right)_{\mathbf{nr}}\right]}{\left(\boldsymbol{\phi}_{\boldsymbol{\varepsilon}}^{1}\right)_{\mathbf{nr}} - \left(\boldsymbol{\phi}_{\boldsymbol{\varepsilon}}^{2}\right)_{\mathbf{nr}}}. \tag{19}$$

In this work, three piezoelectric strain sensors are surface bonded to each candidate location on the structure. The modal principal strains are calculated for sensitivity analysis to predict the increment-decrement effect of the target response by changing the stiffener thickness. Also, the most effective arrangement for stiffener is decided by the principal angle.

3. Numerical Simulation

To examine the validity of the proposed method, finite element analysis is carried out, and the increment-decrement tendency acquired by sensitivity analysis with strain measurement is compared with the FRF changes by local change of thickness. The numerical simulation is based on a thin plate model shown in Figure 4. The length, height, and width of the plate are specified as 400 mm × 500 mm × 3 mm. The analysis model consists of 546 nodes with 500 elements. The boundary condition is set to free-free. The material of the plate and stiffener is stainless steel SUS304. Young's modulus and Poisson's ratio are taken as 197 GPa and 0.3, respectively. The density is taken as 8000 kg/m^3. The principal strain FRFs on each node are used to estimate stiffness sensitivities. The compliance FRFs on each node are used to estimate mass sensitivities. The covering area of stiffener is 20 mm × 20 mm. The stiffener thickness is set as 10^{-1} mm.

The acceleration FRF between the excitation point f and the response point r is shown in Figure 5. Based on the natural mode analysis results shown in Figure 6, a simple twist mode (mode order 7 at 23.98 Hz), a simple bending mode (mode order 8 at 30.19 Hz), a complex twist mode (mode order 14 at 114.13 Hz), and a complex bending mode (mode order 15 at 135.26 Hz) are chosen as target.

The principal strain distributions of four natural modes are shown in Figure 7. The maximum principal strains are shown in red, and the minimum principal strains are shown in blue. It can be seen that on the free edge of plate or at the node of some mode, there is a

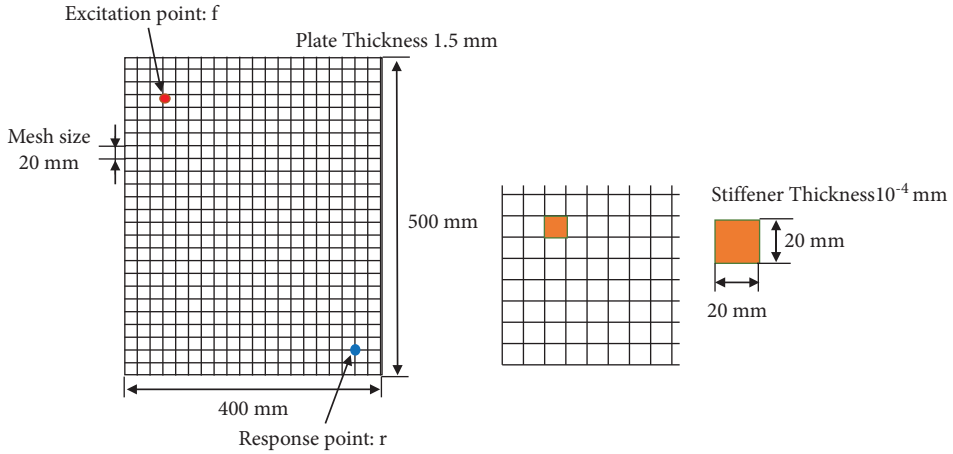

Figure 4: Plate model and stiffener.

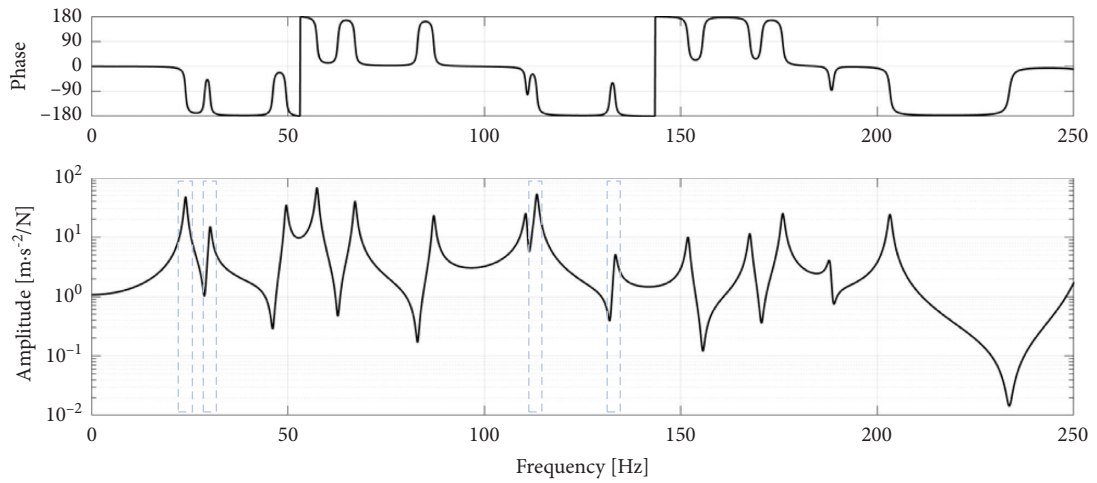

Figure 5: Acceleration FRF at the evaluation point.

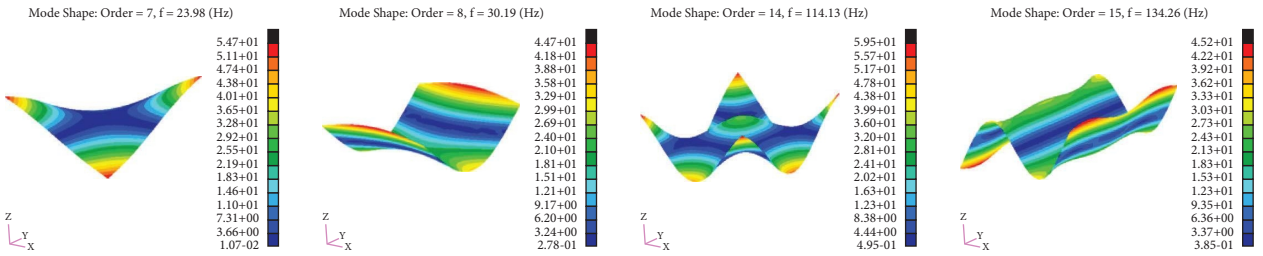

Figure 6: Normal mode analysis results.

smaller value of principal strain since the local transformation is smaller. Also, on the anti-node of some modes, there is a greater value since the local transformation is larger. In the case of twisting mode, in the greatest deformation region, the maximum principal strain is almost the same with the minimum principal strain. In the case of bending mode, in the greatest deformation region, the maximum principal strain is along the bending direction, and the minimum principal strain is almost zero.

Stiffness sensitivity analysis with principal strain measurement is carried out around the target peak frequency. The selected frequency is taken at 23 Hz (simple twisting mode), 29.2 Hz (simple bending mode), 113.1 Hz (complex twisting mode), and 133.2 Hz (complex bending mode). They are 1 Hz less than each peak

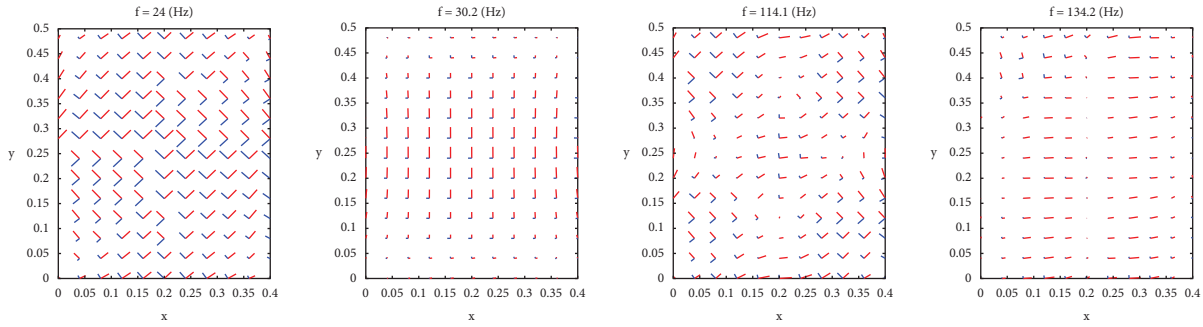

Figure 7: Principal strain arrangements of four natural modes.

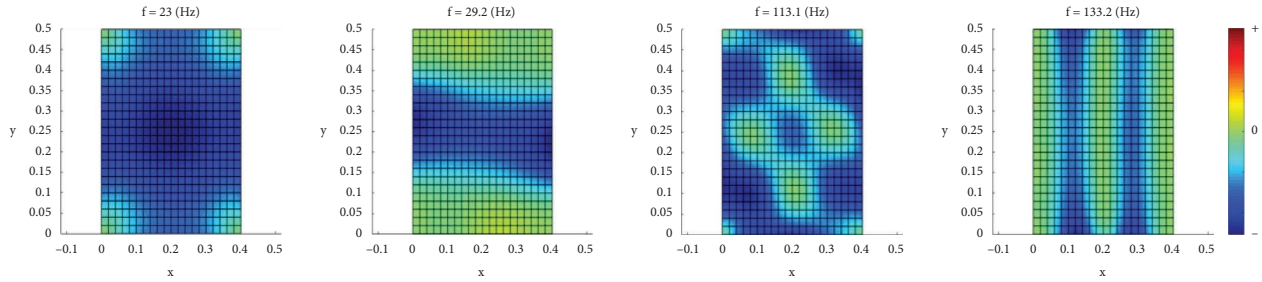

Figure 8: Stiffness sensitivity analysis at four chosen frequencies.

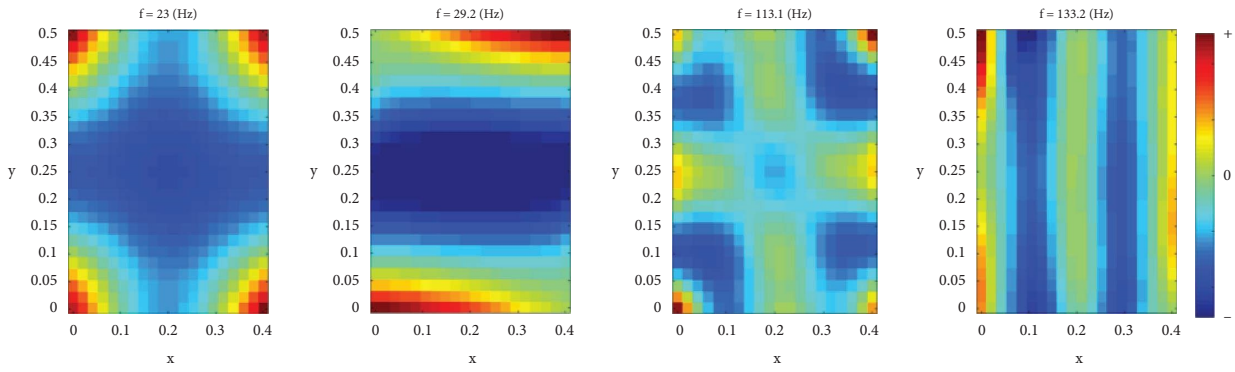

Figure 9: FRF changes by local thickening at four chosen frequencies.

frequency since the peak of FRF is close to the pole, the tendency and value of sensitivity are extremely changing, and the prediction accuracy of the sensitivity is limited.

The increment-decrement tendencies acquired by stiffness sensitivity analysis are shown in Figure 8. The decrement tendencies are shown in blue, which means that the target FRF will decrease by attaching stiffener at each quad element. The FRF changes at four chosen frequencies by local thickening are shown in Figure 9. Whether the chosen peak frequency corresponds the bending modes or twisting modes, the FRF changes are essentially consistent with the tendency acquired by sensitivity analysis at four chosen frequencies. The increment region as shown in red cannot be seen in the stiffness sensitivity results due to the increment caused by mass attachment. It can also be confirmed by the mass sensitivity results shown in Figure 10.

4. Experimental Validation

The validity of the proposed method is also examined by an experimental approach. We used the same stainless plate model in numerical simulation as shown in Figure 11. The length, height, and width of the plate are specified as 400 mm × 500 mm × 3 mm. The boundary condition is assumed to be free-free: the specimen is softly suspended. FFT spectrum analyzer is used to obtain the FRFs between the strain response and force excitation in the frequency range of 0–800 Hz with frequency resolution of 0.6125 Hz. An impact hammer (086C01, PCB) is used to apply the impact force to the plate at excitation point, and a piezoelectric strain sensor (740B02, PCB) and accelerometer (352C65, PCB) measure the response at 5 candidate locations (shown in green dot) and one response point (on the bottom-right corner). Limited by the amount of strain sensors, the

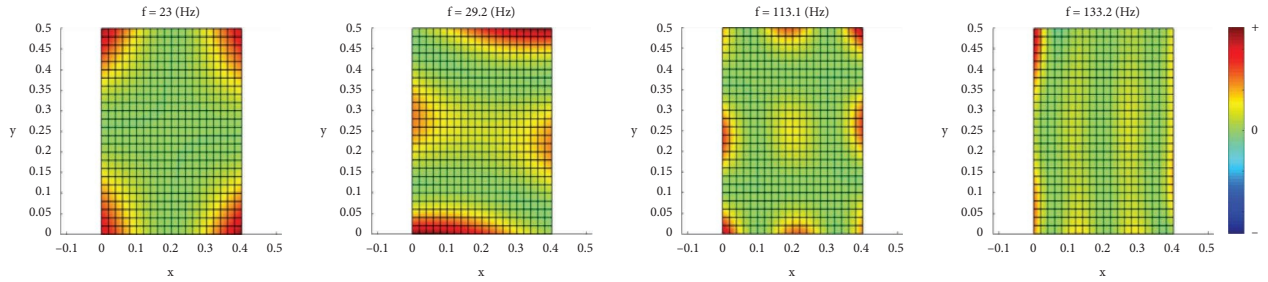

Figure 10: Mass sensitivity analysis at four chosen frequencies.

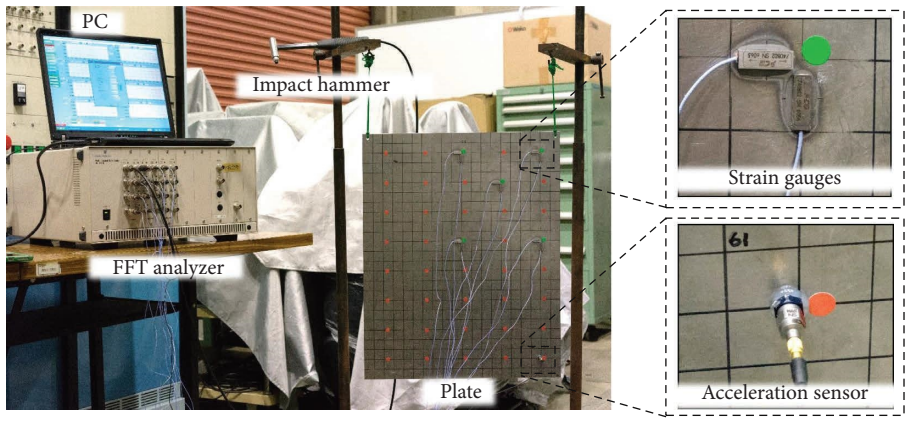

Figure 11: Experiment overview.

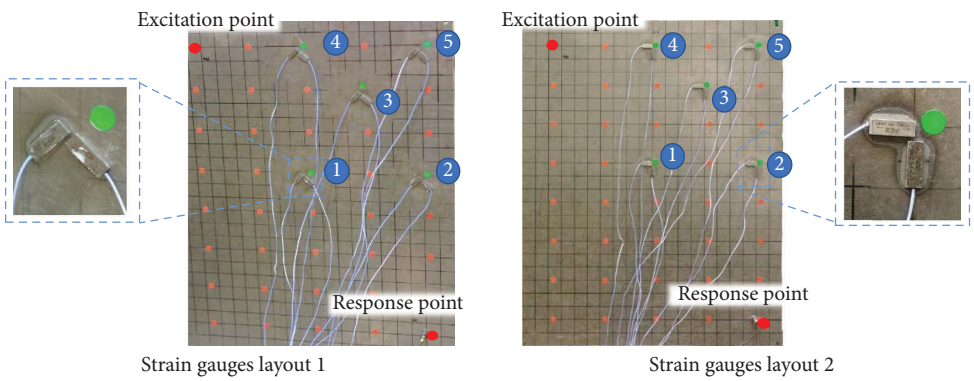

Figure 12: Two strain sensors' layouts.

experiment was carried out in two arrangements. The detailed layouts are shown in Figure 12. The experiment data in two layouts were used to calculate the maximum principal strain FRFs on 5 locations and then used to calculate the stiffness sensitivity.

Stiffness sensitivity analysis with principal strain measurement was also carried out at 1 Hz less than each peak frequency. The selected frequency was taken at 22.9 Hz (simple twisting mode), 29.8 Hz (simple bending mode), 113.5 Hz (complex twisting mode), and 141.2 Hz (complex bending mode). The experimental results are shown in Figure 13. It can be seen that the results are basically consistent with the simulation results. To have a better performance in all four modes and considering the influence of mass attachment, candidate location 3 is chosen to add a stiffener.

The stiffener size is 80 mm × 40 mm × 0.8 mm, and it is made by stainless steel SUS304. It was attached to the plate as shown in Figure 14 by metal adhesive (Devcon A). Target FRF before and after modification is shown in Figure 15. The result shows an overall peak reduction at 4 selected frequencies, which is consistent with sensitivity analysis results. But it also should be pointed out that the metal adhesives might cause a considerable attenuation effect on the peaks over 70 Hz. In order to minimize the attenuation effect, the target FRF before and after modification is processed by

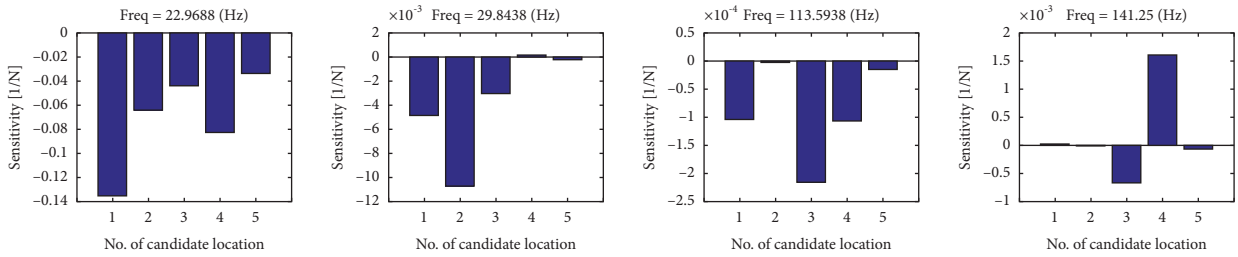

Figure 13: Experimental stiffness sensitivity analysis at four chosen frequencies.

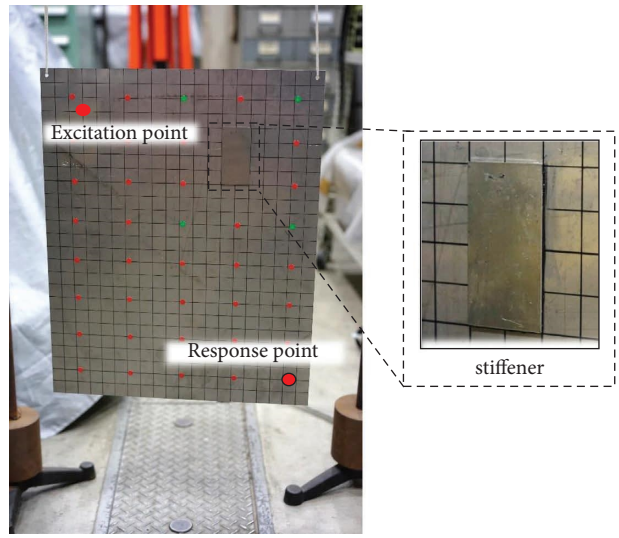

Figure 14: Plate with stiffener attachment.

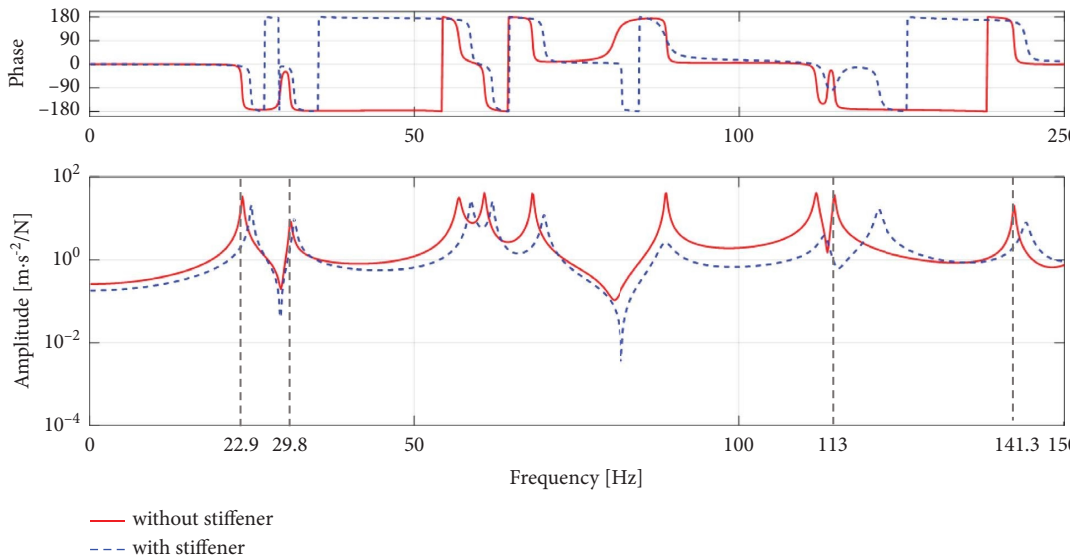

Figure 15: Target FRF before and after modification.

curve fitting with same modal damping ratio as shown in Figure 16. The result shows an overall peak shift to higher frequency range by stiffener attachment, and this also makes a downward trend at 4 selected frequencies marked at frequency axis. The most remarkable peak shift and decrement happened at third selected frequency (113 Hz) since

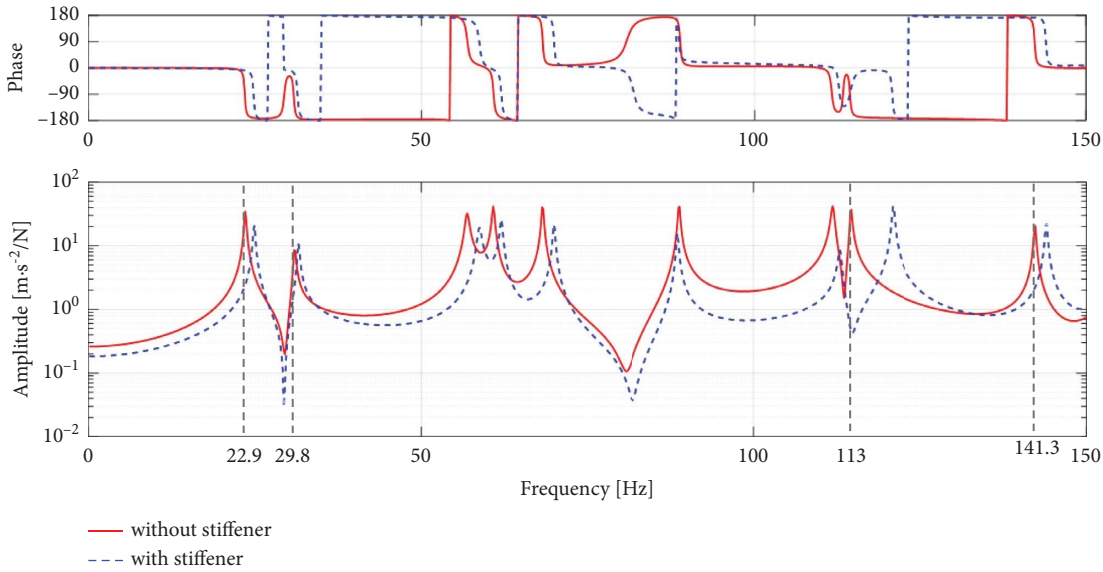

Figure 16: Target FRF before and after modification (with same modal damping ratio).

the stiffener effectively increases local stiffness. The first selected frequency (22.9 Hz) and fourth selected frequency (141.3 Hz) also show an obvious peak shift and decrement, while there is no appreciable peak shift and decrement at the second chosen frequency (29.8 Hz) because the effects of additional stiffness and additional mass cancel each other out at location 3.

Overall, the experimental results are basically consistent with the sensitivity results. It can be effectively applied to find the modification location on the structure to make a remarkable decrement of response at the target frequency. There will be a further reduction effect if consider the damping effect of metal adhesives.

5. Conclusion

This paper introduced a stiffness sensitivity analysis with principal strain measurement to decrease the out-of-plane vibration, which is the main cause of the sound radiation of mechanical structures. The validity of the proposed method was examined through numerical simulation with a FEM model of the plate structure. The modal principal strain distribution based on twisting mode and bending mode was discussed. Stiffness sensitivities were calculated and checked with FRF changes by local thickening at 4 selected frequencies. It was also examined by the experimental approach. The expected reduction of the response is attained by adding the stiffener (a thin stainless plate) to the appropriate location on the plate. In summary, the simulations and experiments validated the correctness of applying principal modal strain to sensitivity analysis. Therefore, it can be used as a quick optimization design tool for mechanical structures with plate components.

Data Availability

The data used to support the findings of this study are available from the corresponding author upon request.

Conflicts of Interest

The authors declare that they have no conflicts of interest.

References

[1] W. J. Joost, "Reducing vehicle weight and improving U.S. Energy efficiency using integrated computational materials engineering," *Journal of Occupational Medicine*, vol. 64, no. 9, pp. 1032–1038, 2012.

[2] M. N. Zadeh and S. V. Sorokin, "Simplified description of out-of-plane waves in thin annular elastic plates," *Journal of Sound and Vibration*, vol. 332, no. 4, pp. 894–906, 2013.

[3] H. Lee and R. Singh, "Acoustic radiation from out-of-plane modes of an annular disk using thin and thick plate theories," *Journal of Sound and Vibration*, vol. 282, no. 1-2, pp. 313–339, 2005.

[4] I. Ramli, Z. Nuawi, S. Abdullah et al., "The study of EMA effect on modal identification: a review," *Journal of Mechanical Engineering and Technology*, vol. 9, no. 1, pp. 103–121, 2017.

[5] S. H. Kim, J. M. Lee, and M. H. Sung, "Structural-acoustic modal coupling analysis and application to noise reduction in A vehicle passenger compartment," *Journal of Sound and Vibration*, vol. 225, no. 5, pp. 989–999, 1999.

[6] K. Terada and T. Yoshimura, "Sensitivity analysis for noise reduction under operational State(<Special Issue>Dynamics & design conference 2009)," *Transactions of the Japan Society of Mechanical Engineers Series C*, vol. 76, no. 765, pp. 1331–1337, 2010.

[7] SG. Ye, L. Hou, PD. Zhang et al., "Transfer path analysis and its application in low-frequency vibration reduction of steering wheel of a passenger vehicle," *Applied Acoustics*, vol. 157, p. 107021, 2020.

[8] Y. Nakamura, T. Yoshimura, and G. Tamaoki, "Sensitivity analysis using bending stiffness of panel structures vibration analysis by the scanning laser Doppler vibrometer," *Dynamics & Design Conference*, vol. 125, 2010.

[9] Y. Tsurumi, T. Nakagawa, N. Mori, and H. Yamakawa, *Transactions of the Japan Society of Mechanical Engineers, Series C*, vol. 67, no. 663, pp. 3421–3427, 2001.

[10] S. Doebling, F. Hemez, M. Barlow et al., *Selection of Experimental Modal Data Sets for Demage Detection via Model Update*, 34th Structures, Structural Dynamics and Materials Conference, Jolla,CA,USA, 1993.

[11] K. Yamada, T. Yoshimura, and S. Moromi, *Reduction of Noise and Vibration by Sensitivity Analysis of Stiffness Modification with Strain Measurement*, Dynamics & Design Conference, Cavtat, Dubrovnik, Croatia, 2016.

[12] L. R. Ray, B. H. Koh, and L. Tian, "Damage detection and vibration control in smart plates: towards multifunctional smart structures," *Journal of Intelligent Material Systems and Structures*, vol. 11, no. 9, pp. 725–739, 2000.

[13] K. Terada and T. Yoshimura, "Sensitivity analysis of time history response for structure modification," *JSAE Annual Congress (Spring)*, vol. 262, 2014.

[14] O. C. Zienkiewicz and R. L. Taylor, *The Finite Element Method for Solid and Structural Mechanics*, Elsevier, Oxford, UK, 2005.

[15] Y. Zhou, S. Wu, N. Trisovic, Q. Fei, and Z. Tan, "Modal strain based method for dynamic design of plate-like structures," *Shock and Vibration*, vol. 2016, pp. 1–10.

[16] D. Emad, M. A. Fanni, and A. M. Mohamed, "Comparison of uniaxial and triaxial rosette gages for strain measurement in the femur," *JSAE Annual Congress (Spring)*, vol. 262, 2014.